A MICROEARTHQUAKE STUDY OF THE FRACTURE STRUCTURE IN THE TAKINOUE GEOTHERMAL AREA

SUGIHARA Mituhiko and Toshiyuki TOSHA
Geol. Surv. of Japan, Higashi 1-1-3, Tsukuba 305, Japan

1. Introduction

This paper describes promising methods for analyzing microearthquake data which potentially can resolve underground fracture structures to accuracies of the order of ten meters. We have been observing microearthquake activity of microearthquakes in the Takinoue geothermal area in the vicinity of the Kakkonda geothermal power plant, Iwate Prefecture, Northeast Japan (Figure 1) since December 1982. In this area, high temperature fluid rises through fractures which penetrate a hot body of intrusive rock (Ide,1985). The shape of the Matsuzawa intrusive rock formation was recently established primarily by core sample analysis (Doi et al.,1988) (Figure 2).

We determined hypocenter locations of numerous microearthquakes recorded by eight permanent stations and seven temporal stations (Figure 2) during a pressure build-up test which took place in June,1985. Many microearthquake hypocenters were located within the Matsuzawa intrusive rock formation (Figure 2). These microearthquakes (hereafter designated "Matsuzawa microearthquakes") are presumably associated with fractures within the intrusive rock.

2. Hypocenter and focal mechanism

Each particular station is characterized by a particular waveform that is observed for each of the Matsuzawa microearthquakes; see Figure 3, for example. This common waveform pattern permits more accurate assessment of P-wave arrival times for the various microearthquakes, particularly for weak and/or overlapping events. This analysis revealed that many of the hypocenters were located along a NNW-SSE trending vertical plane (Figure 4). Focal mechanism solutions indicate both reverse and strike-slip fault type solutions along a common E-W P-axis (Figure 5).

3. Source process analysis

If the rupture duration (T1) of a microearthquake is extremely small compared to the impulse response time due to attenuation (T2) (figure 6), the source-time function of a small microearthquake can be treated as a delta function; the waveform of the microearthquake can be treated as the empirical Green's function which represents the effects of both (1)wave propagation through heterogeneous media and (2)recording system response. Expressing the waveform of the larger microearthquakes as the convolution of the proper source-time function and the empirical Green's function, we can analyze the microeartquake source process (Frankel and Kanamori,1983). This method avoids the difficulty of directly analyzing the complicated waveform resulting from heterogeneous crustal structure (Figure 6).

We used this method to analyze the largest of the Matsuzawa microearthquakes (the fourth record in Figure 3; hereafter called the "mainshock"). For the Green's function, we used the waveform of the aftershock which occured immediately after the mainshock because; (1)both the hypocenter and the focal mechanism of this aftershock are almost the same as those of the mainshock (Figure 5), (2)the signal-to-noise ratio is high, and (3)the waveform similarity between this aftershock and the other smaller microearthquakes indicates that the source process of this aftershock is the same as that of the smaller events.

For each station we assumed a source-time function consisting of a single pulse of duration T (Figure 7). We calculated the waveforms for various values of T; compared them with the waveform of the mainshock, and selected the value which produced computed waveform most similar to the observed mainshock as the apparent rupture duration (Figure 7). Figure 8 shows the values of T obtained at each station. The apparent rupture duration is long near station JM8 and short near station GS1. This trend indicates the rupture direction; since this direction coincides with the strike of one nodal plane of the focal mechanism solution, we infer that the ruputure propagated in the ENE direction along the vertical plane as shown in Figure 8.

Because GS5 and GS6 are located perpendicular to the inferred rupture plane, the apparent rupture durations at GS5 and GS6 should represent the true rupture duration. The length of the fault along which this microearthquake occured can be estimated by multiplying the rupture duration T by the rupture velocity Vr. Assuming Vr = 0.9Vs = 2.2 km/s, we obtain the length of the fault L:

$L = T \times Vr = 0.014 \text{ sec} \times 2200 \text{ m/sec} \cong 30 \text{ m}$

4. Fracture structure

Taking the direction of the rupture plane of the mainshock to be ENE-WSW, we can interpret the spatial distribution of focal mechanism solutions (Figure 5) more explicitly.

If all the strike-slip microearthquakes have the same ENE-WSW rupture plane orientation as the mainshock, they appear to connect the en-echelon array of reverse faulting type microearthquakes (Figure 9). The distribution of P-axes and T-axes of the focal mechanism solutions (Figure 5b) shows that local and regional stress fields coincide. Under these circumstances, the fault pattern shown in Figure 9 is plausible.

The hypocenter distribution indicated the presence of a NNW-SSE trending vertical fracture within the Matsuzawa intrusive formation (Figure 4). If the fracture is a single planar reverse fault, it must be relatively impermeable owing to the compressional stress field. If, however, the fracture consists of a series of small faults as indicated in Figure 9, the compressive stress may be sustained without pore closure, and the fracture zone may consequently be very permeable. That is, a small strike-slip fault such as the source fault for the "mainshock" studied here could result in a permeable reverse fault structure.

5. Conclusions

Precise analysis of the microearthquake signals has provided a clear hypocenter distribution which is characterized by the NNW-SSE trending vertical plane which consists of a series of small faults. These results have provided an accurate delineation of the fracture structure which was previously unavailable. We conclude with a few observations concerning the analysis and the data upon which it is based.

(a) As shown in Figure 3, at station GS5 , there is a strong signal 0.1 second after the P-wave arrival. This later feature is believed to be the same wave reflected at the source region for the following reasons (1) Station GS5 situated on exposed rock, so the effects of surface reflection can probably ruled out. (2) Similar late feature can be discerned at station GS3 (Figure 7b). (3) The direct wave is weak at GS5 because of the source radiation pattern. If the late feature is a reflected wave which was radiated from the source in another direction, the greater strength of the late feature (compared to the first motion) may be explained. Other late features are also detected at some stations. Analysis of variations of these features from station to station and/or from event to event may shed light on the location and characteristics of the reflector/scatterer.

(b) In this paper we determined hypocentral locations assuming a layered velocity structure and using the HYPO71 program (Lee and Lahr,1975). More sophisticated methods might provide a clearer hypocenter distribution. First motion particle motion directions are somewhat at variance with the station/source geometry, which suggests that three-dimensional ray tracing should really be used to locate hypocenters.

(c) In order to analyze the source process properly, the empirical Green's function should be integrated both in space and in time, and the response at all stations should be modeled simultaneously. Such an approach should reveal more detailed fracture structures.

(d) The clarity of the first motion records obtained at station GS3 (Figure 7b) permitted us to estimate the seismic moment of the mainshock to be 5×10^{16} dyne-cm. The mainshock stress drop was estimated to be 10 bars. Although not conclusive, this suggests that it may be possible to use empirical earthquake source correlation to estimate the dynamics of fractures.

Acknowledgements -- Discussions with Dr. Nobuo Doi and Mr. Masayuki Tateno of Japan Metals and Chemicals Co., Ltd. were very helpful. We acknowledge the effort of Dr. Hisao Ito of Geological Survey of Japan in planning, installing and supervising the Takinoue seismic network. We also thank Drs. Hitoshi Kawakatsu and Koichi Nakamura for critically reviewing this manuscript.

References

Doi,N., Kudo,H., Takanohashi,M. and Niitsuma,H. (1988) AE Measurement and Fracture Behavior during Hydraulic Fracturing in the Kakkonda Geothermal Field, Japan., J. Geothermal Res. Soc. Japan., 10, 237-249.

Frankel,A. and Kanamori,H. (1983) Determination of Rupture Duration and Stress Drop for Earthquakes in Southern California., Bull. Seism. Soc. Am., 73, 1527-1551.

Ide,T. (1985) Geothermal Models of the Matsukawa and Kakkonda areas., J. Geothermal. Res. Soc. Japan., 7, 201-213.

Ito,H. and Sugihara,M. (1987) Earthquake Data Aqusition System in the Takinoue Geothermal Area., Bull. Geol. Surv. Japan, 38, 247-264.

Lee,W.H.K. and Lahr,J.C. (1975) HYPO71 (Revised) : A Computer Program for Determining Hypocenter, Magnitude, and First Motion Pattern of Local Earthquakes., U.S.G.S. Open File report, 75-311.

Urabe,T. (1982) Spectral Characteristics of Microearthquakes Occuring Concentratedly in Time and Space., Master Thesis of the Univ. of Tokyo, 1-96.

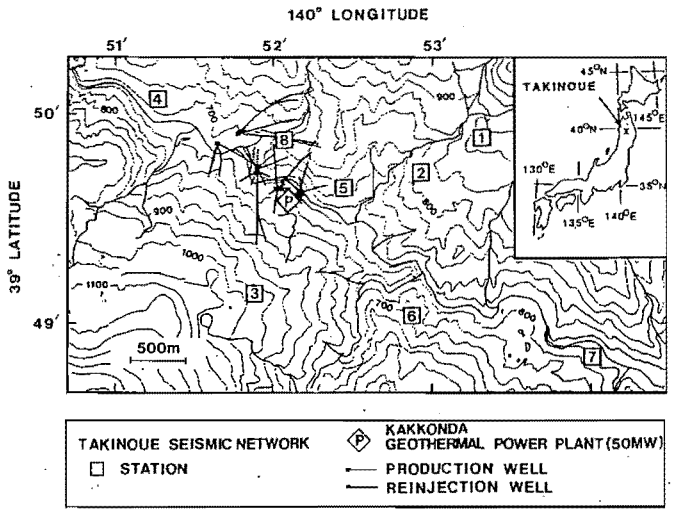

Figure 1.
Location of the Takinoue geothermal area. The eight-station seismic network has been deployed since December, 1982. Microearthquake waveforms are recorded in digital form by 500 Hz sampling (Ito and Sugihara,1987).

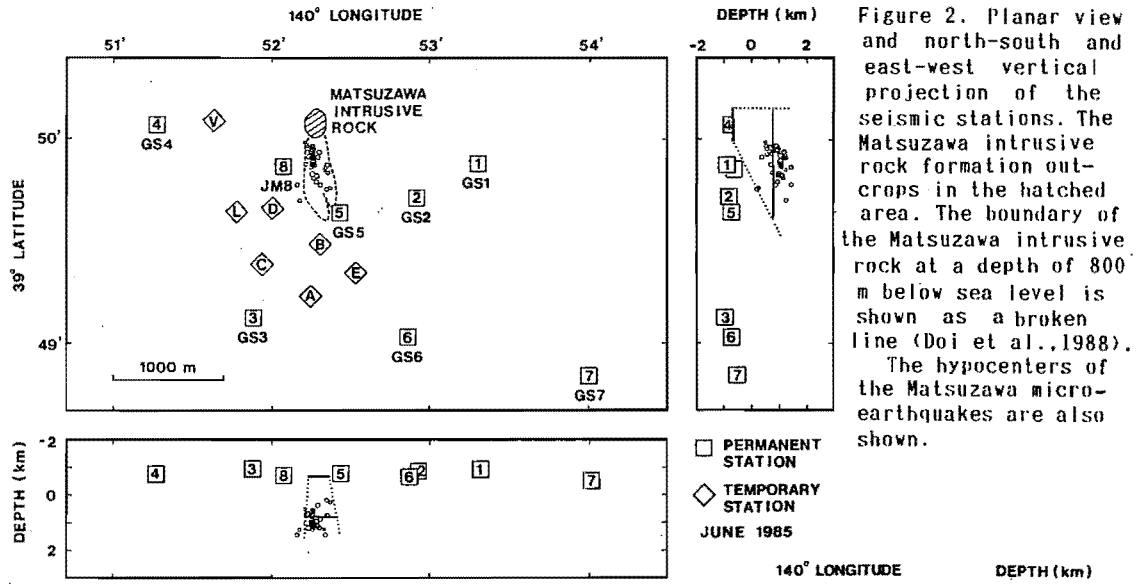

Figure 2. Planar view and north-south and east-west vertical projection of the seismic stations. The Matsuzawa intrusive rock formation outcrops in the hatched area. The boundary of the Matsuzawa intrusive rock at a depth of 800 m below sea level is shown as a broken line (Doi et al.,1988).
The hypocenters of the Matsuzawa microearthquakes are also shown.

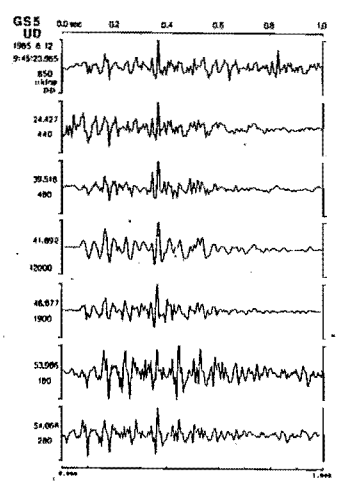

Figure 3.
Waveforms of the Matsuzawa microearthquakes recorded at station GS5.

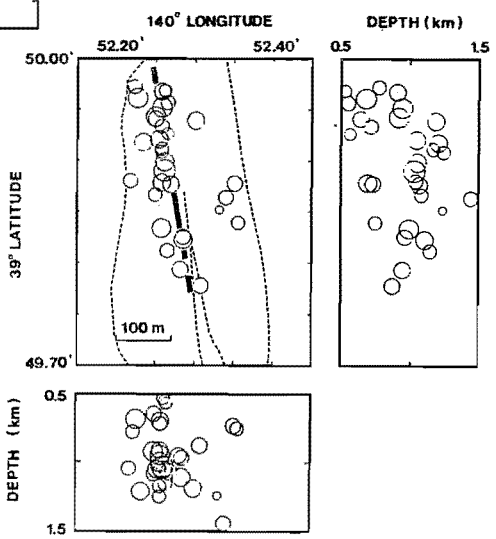

Figure 4. Microearthquake hypocenter distribution in the center part of the Matsuzawa intrusive rock formation.

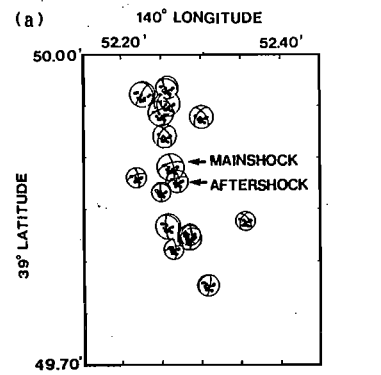

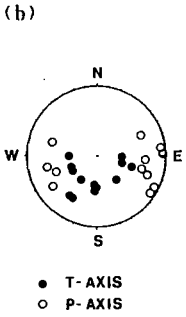

Figure 5.
(a) Distribution of focal mechanism solutions of the Matsuzawa microearthquakes.
(b) Distribution of P-axes and T-axes of the Matsuzawa microearthquakes.

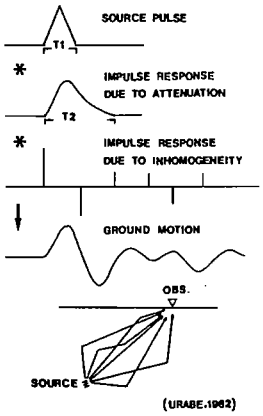

Figure 6. Interpretation of complex microearthquake waveform. Ground motion at the seismic station is assumed to be convolution of source pulse, impulse response due to attenuation, and impulse response due to inhomogeneity (Urabe,1982).

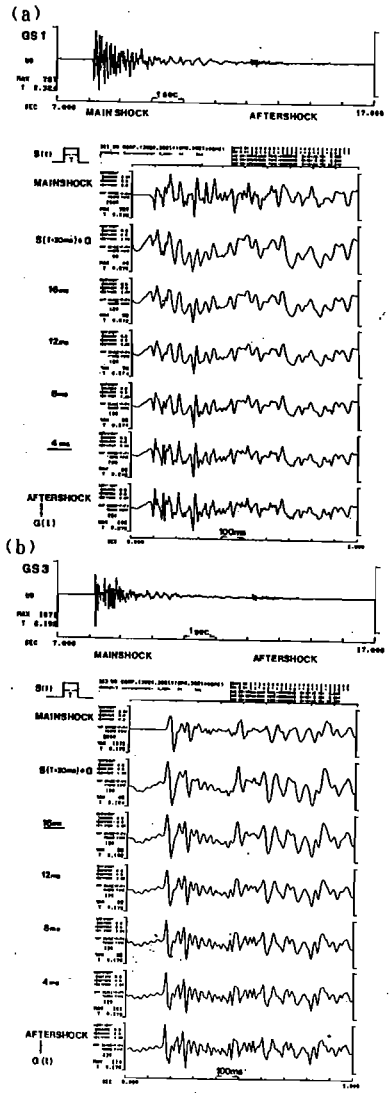

Figure 7. Waveforms of mainshock and aftershock recorded at GSI (Figure 7a) and at GS3 (Figure 7b). Waveforms synthesized by convolution of the empirical Green's function (waveform of the aftershock) and various source-time functions are also shown for comparison.

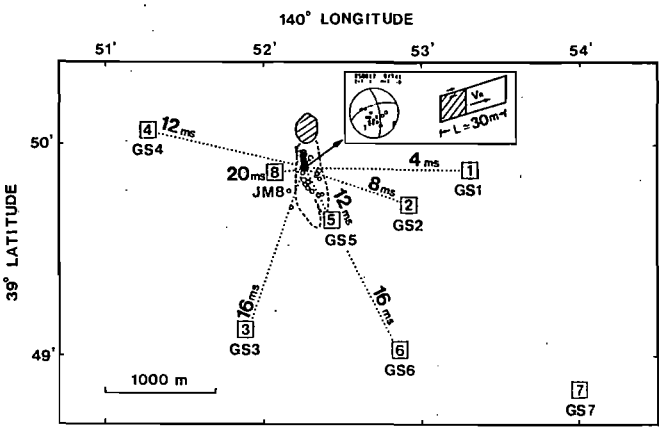

Figure 8. Distribution of apparent rupture durations and the estimated rupture plane.

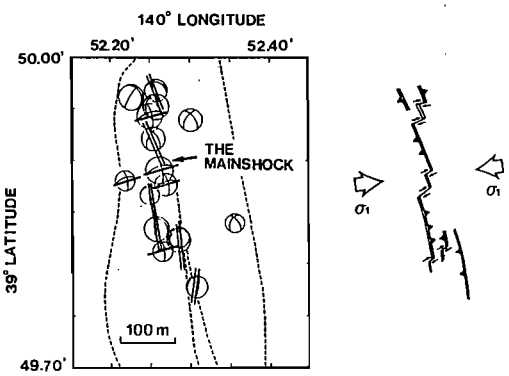

Figure 9.
Interpretation of focal mechanism solutions.